©2009 Society of Economic Geologists, Inc.
Economic Geology, v. 104, pp. 351–363

Rb-Sr Geochronology of Chalcopyrite from the Chehugou Porphyry Mo-Cu Deposit (Northeast China) and Geochemical Constraints on the Origin of Hosting Granites

Bo Wan,[1,2,†] Ernst Hegner,[2] Lianchang Zhang,[1] Alexander Rocholl,[3]
Zhiguang Chen,[1] Huaying Wu,[1] and Fukun Chen[1]

[1] *Key Laboratory of Mineral Resources, Institute of Geology and Geophysics, Chinese Academy of Sciences, PO Box 9825, Beijing, China*

[2] *Department of Earth and Environmental Sciences, Universität München, Luisenstr. 37, München, Germany*

[3] *Department of Earth and Environmental Sciences, Universität München, Theresienstr. 41, München, Germany*

Abstract

The Chehugou porphyry Mo-Cu deposit is located ca. 300 km north of Beijing in the boundary zone between the Archean North China craton and the Neoproterozoic-Mesozoic Central Asian orogenic belt. Using hydrothermal chalcopyrite from this deposit, we are able to show for the first time that the Rb-Sr isotope system in massive, nonfractured chalcopyrite grains can provide reliable age constraints for Mo-Cu deposits. We analyzed two chalcopyrite samples from slightly different petrogenetic "environments" showing contrasting texture and deformation history. Five 2- to 5-mg fragments of a single nonfractured chalcopyrite grain containing spatially isolated inclusions of K-mica, K-feldspar, and quartz yielded an Rb-Sr isochron age of 256 ± 7 Ma (2σ including λ uncertainty). For this sample, the dense chalcopyrite "matrix" apparently inhibited diffusion of Rb and Sr after chalcopyrite crystallization, and the age should therefore reflect the time of crystallization of chalcopyrite from the Mo-Cu mineralizing fluids. The evidence for Mo-Cu mineralization during the late Permian requires a revision of the previous notion that the Chehugou deposit was formed during the Yanshanian orogeny lasting from 200 to 60 Ma.

Fragments of a second chalcopyrite sample that, in contrast to the first, had experienced deformation as indicated by intragranular fractures and alignment of K-mica and K-feldspar inclusions along these fractures. This sample yielded a clearly younger Rb-Sr isochron age of 207 ± 15 Ma (2σ). This age obviously reflects an isotopically open system due to fluid movement and/or prolonged diffusion of Rb and Sr along the fractures. Single biotite crystals from an associated monzogranite yielded an Rb-Sr isochron age of 250 Ma, which is interpreted as a lower age limit for the Mo-Cu mineralization, and the time when the granite cooled below 400° to 300°C. Considering the field evidence for a broadly contemporaneous origin of the Mo-Cu mineralization and the hosting granitoids, we suggest that the granitoids are not much older than ca. 260 Ma.

The Mo-Cu–hosting granitoids range in composition from monzogranite to highly evolved syenogranite with high La/Yb and Sr/Y ratios. Initial ε_{Nd} values of ca. –21 to –23 (Nd crustal residence times of the sources 1.9 to 2.7 Ga) indicate melting of the predominantly Archean North China craton, and a subordinate juvenile mantle-derived component. Much older U-depleted lower crustal sources for the granitoids are supported by high initial $^{208}Pb/^{204}Pb$ ratios. Lithospheric delamination and underplating of hot mantle-derived material may have facilitated crustal melting in a late orogenic to postcollision.

Introduction

In the Chifeng area of Inner Mongolia (northeast China, Fig. 1) up to 14 Mo-Cu deposits have been discovered in the last 20 years (Tang, 1990; Bureau of Geology and Mineral Resources of Inner Mongolia, BGMRIM, 1991; Hsu et al., 1991; Davis et al., 2001). In spite of their economic importance, the temporal framework of mineralization and origin of the host rocks as well as the nature of mineralizing fluids have not been investigated to date. Among these deposits, Chehugou is the largest and most representative porphyry Mo-Cu deposit (Figs. 1, 2). In this paper we document the suitability of the Rb-Sr isotope system in individual chalcopyrite grains from the Chehugou deposit for constraining the age of Mo-Cu mineralization. Using Nd and Pb isotope and geochemical data we elucidate the sources of the Mo-Cu–hosting granitoids and suggest a tectonic setting for the deposit.

Geochronological Strategy

Age determinations of ore minerals using the Rb-Sr system in mineral or fluid inclusions in sulfide minerals have been successfully carried out for almost two decades (Nakai et al., 1990; Christensen et al., 1995; Yang and Zhou, 2001; Li et al., 2008a). Most of these studies focused on sphalerite and pyrite, but to our knowledge, Rb-Sr dating of very small (<5 mg) fragments of chalcopyrite grains, as has been performed in this study, has not been attempted before. Li et al. (2008a) noted that for sulfide samples from the hydrothermal gold deposits from the Jiaodong area, China, large variations of Rb and Sr concentrations were caused by inclusions of silicate minerals, especially hydrothermal K-mica and K-feldspar. If Sr isotope equilibrium between individual mineral and/or fluid inclusions had been achieved during hydrothermal activity and isotopic exchange between them did not occur after their formation, the Rb/Sr ages should be meaningful with respect to the formation of the ore minerals and the deposit (Li et al., 2008a).

In previous studies, the very low concentrations of Rb and Sr in sphalerite and pyrite proved to be an analytical challenge so that large samples up to 100 mg had to be handpicked and chemically processed. It was realized that large samples showed a tendency for preservation of isotopic disequilibrium between mineral and fluid inclusions. This condition typically

† Corresponding author: e-mail, Wanbo@mail.iggcas.ac.cn

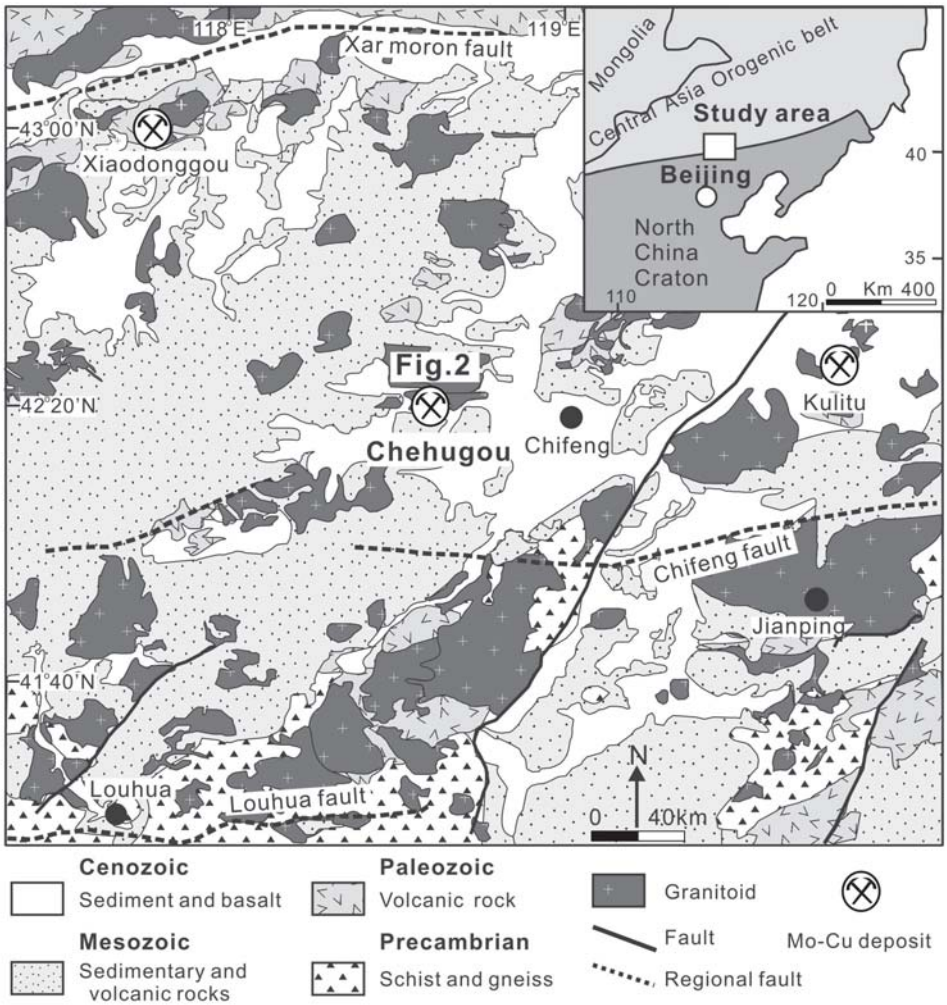

FIG. 1. Geologic map of Chifeng area showing the major lithological units and faults. The localities of the Mo-Cu deposits including the Chehugou mine are indicated. Source: Map of the Bureau of Geology and Mineral Resources of Inner Mongolia (BGMRIM, 1991).

resulted in errorchrons, making it difficult to infer geologically meaningful ages (e.g., Christensen et al., 1995). On the other hand, it has been shown earlier for pyrite that on a small sample scale, Rb-Sr isotope equilibrium has often been reached (Li et al., 2008a).

In this study we tried to avoid the potential problem of isotopic disequilibrium by analyzing very small fragments of chalcopyrite grains (<5 mg), handpicked from single small and crushed chalcopyrite chips.

Geologic Framework of Study Area

The Chifeng region—comprising up to 14 Mo-Cu deposits, including the Chehugou deposit—is situated in the central part of a boundary zone between the Archean North China craton and the Neoproterozoic-Mesozoic Central Asian orogenic belt (Fig. 1). The boundary zone comprises a wide range of lithologic-tectonic units such as Precambrian continental fragments, late Paleozoic island-arc assemblages, Mesozoic continental volcanosedimentary successions, and crosscutting late Paleozoic to late Mesozoic granitoids (Tang, 1990; Davis et al., 2001; Xiao et al., 2003; Wu et al., 2005; Zhang et al., 2007, 2009). The youngest rocks with typical subduction-related characteristics are of late Carboniferous age (Zhang et al., 2007) and the oldest postcollision intraplate igneous rocks are middle to late Mesozoic (Davis et al., 2001; Wu et al., 2002; Zhang et al., 2009). This relationship suggests that the Paleo-Asian Ocean closed sometime during the late Paleozoic to early Mesozoic. The U-Pb zircon age spectrum for granitoids suggests three major igneous events lasting from 311 to 304 Ma (Zhang et al., 2007, 2009), 253 to 237 Ma (Chen et al., 2000; Davis et al., 2001), and 143 to 135 Ma (Chen et al., 2003; Li et al., 2003). Geochemical and isotopic data of the ca. 300 Ma granites support melting of juvenile subduction-related protoliths (Zhang et al., 2007, 2009), as opposed to old lower crustal sources for intraplate syenogranites of ca. 130 Ma (Chen et al., 2003; Li et al., 2003). The granites of ca. 240 to 250 Ma apparently were derived from mixed crustal sources comprising juvenile and older material (Chen et al., 2000; Davis et al., 2001).

The Chifeng region is characterized by east-striking faults that are cut by northeast-striking faults, all considered to be related to the 200 to 60 Ma Yanshanian orogeny (Bureau of

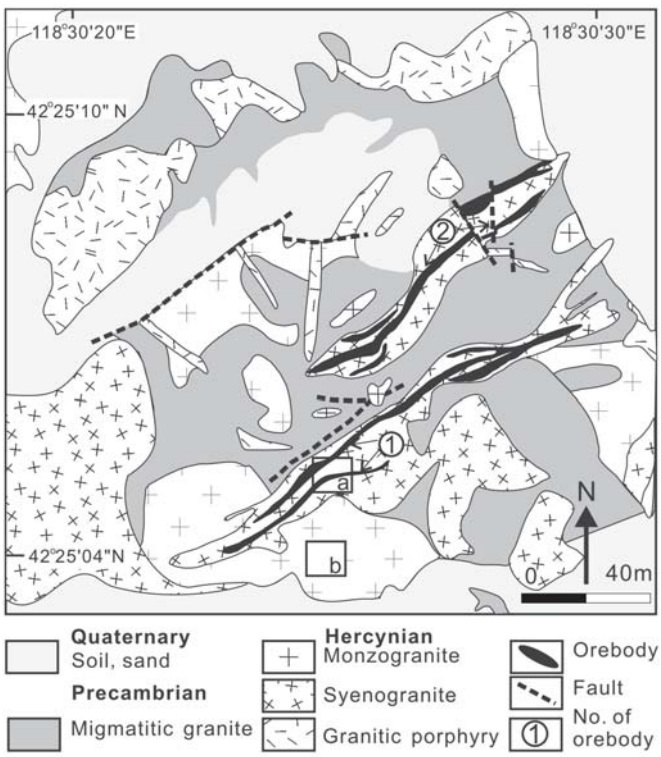

FIG. 2. Geologic map of Chehugou mine with sections of the two orebodies in syenogranite. Sample localities: area "a": chalcopyrite and syenogranite samples CG11 to CG14: 42°25'05"N, 118°30'25"E - 118°30'26"E; area "b": monzogranite samples CG31 to CG34: 42°25'04"N, 118°30'25"E -118°30'26"E. Modified map of BGMRIM (1991).

Geology and Mineral Resources of Inner Mongolia, BGMRIM, 1991). Among the east-striking faults, the Chifeng fault system was recognized as the major lithotectonic boundary between the North China craton and the Central Asian orogenic belt (Tang, 1990; Hsu et al., 1991; Davis et al., 2001; Xiao et al., 2003). Field reports of the Bureau of Geology and Mineral Resources of Inner Mongolia (BGMRIM, 1991) suggested formation of the Chehugou porphyry Mo-Cu deposit during the Yanshanian orogeny (200 to 60 Ma). This inference is, however, not supported by the new radiometric data of this study (see below).

The tectonic setting of the study area during the Paleozoic has been interpreted as a continental arc resulting from the south-directed subduction of the Paleo-Asian Ocean floor from early Silurian onward (Coleman, 1994; Sengör and Natal'in, 1996; Chen et al., 2000; Johnson et al., 2001; Wu et al., 2002; Xiao et al., 2003; Liu et al., 2005). The time frame of the closure of the Paleo-Asian Ocean is being debated as Permian (Tang, 1990; Hsu et al., 1991; Sengör and Natal'in, 1996; Xiao et al., 2003) as well as Carboniferous (Dobretsov et al., 1995; Chen et al., 2000; Zhang et al., 2006, 2007).

Geology of the Chehugou Mine and Description of Samples

The Chehugou mine is located ca. 55 km northwest of the city of Chifeng. The exposed rock types are Precambrian basement with migmatitic granites and intruding Hercynian-age syenogranite, monzogranite, and granitic porphyry (Fig. 2). The area is dissected by major northeast-striking faults that are cut by a set of west- to northwest-striking faults (BGMRIM, 1991).

The major Mo-Cu mineralization is confined to syenogranite, whereas monzogranite shows only low-grade mineralization, which is presently not of economic interest. The observation that syenogranite intrusions follow the older northeast-striking faults may be important with respect to prospecting for other occurrences of high-grade Mo-Cu mineralization. The field evidence for a smooth and irregular contact between the syenogranite and monzogranite suggests contemporaneous intrusion of the bodies in a semiplastic state, a field observation that will be used below to infer the emplacement ages of the Mo-Cu–hosting granites. The Mo reserve of the deposit is ca. 50,000 tons with an average grade of 0.12 percent, and the Cu reserve is ca. 111,000 tons with an average grade of 0.5 percent (BGMRIM, 1991), which classifies the deposit as of small size with respect to global standards (e.g., Seedorff et al., 2005)

The Mo-Cu–bearing pale red syenogranite is mainly composed of microcline, quartz, plagioclase, amphibole, and biotite in decreasing proportions. The monzogranite comprises quartz, plagioclase, orthoclase, amphibole, and biotite. Both rock types contain up to 5 percent modal amphibole. Near the Mo-Cu mineralization, hydrothermal activity led to pervasive K-feldspar alteration and rock silicification. The grade of Mo-Cu mineralization increases with the degree of hydrothermal rock alteration. The alteration zone encompassing the orebody is characterized by sericitization and secondary epidote-chlorite-clay assemblages. Eight samples of syenogranite and monzogranite were chemically and isotopically analyzed for investigation of the mineralizing hydrothermal fluids.

In the Chehugou mine, two subparallel and contemporaneously formed orebodies are associated with a northeast-striking syenogranite intrusion (Fig. 2). Orebody no. 1 in the south extends over a length of ca. 450 m with 1 to 11 m thickness, averaging ca. 4 m; it dips ca. 70°NW. Orebody no. 2 is almost 300 m long with an average thickness of ca. 5 m, also dipping steeply northwest (only sections of the orebodies are shown in Fig. 2). A Re-Os age determined on molybdenite samples from the Chehugou deposit yielded an age of 258 ± 3 Ma (J. Liu, pers. commun., 2007).

The principal ore minerals in the Chehugou mine are molybdenite, chalcopyrite, and pyrite. Molybdenite is mostly disseminated in the host granite but there are also thin coatings of molybdenite on fractures within the host granite. The disseminated occurrence of molybdenite in the host granite supports a close genetic and temporal relationship between ore formation and intrusion and crystallization of the granite magma as has also been documented in other studies of porphyry Mo-Cu deposits (Theodore et al., 1992; Ashleman et al., 1997; Selby et al., 2000; Seedorff et al., 2005).

Chalcopyrite occurs as massive aggregates of irregular shape in fissures of quartz veins and between quartz veins. Individual chalcopyrite aggregates can be up to several centimeters long and up to 1 cm thick. No disseminated or stringer-type chalcopyrite mineralization is seen in hand specimen and thin section. Unlike the molybdenite disseminated in the host granite, the chalcopyrite is closely associated with

quartz veins, which cut through and intrude the host granite. For Rb-Sr age determinations we collected two chalcopyrite samples from two different quartz veins (locality box "a", Fig. 2). Chalcopyrite sample-1 was separated from a quartz veinlet filled with massive chalcopyrite. Under the electron microscope it shows a dense and massive matrix with clearly isolated mineral inclusions (Fig. 3A). Chalcopyrite sample-2, collected from a fractured stockwork zone, shows under the electron microscope brittle deformation characteristics with inclusions of silicate minerals concentrated along fractures. Representative semiquantitative SEM analyses of the mineral inclusions are listed in Table 1. The Si, Al, Mg, Fe, and K concentrations suggest K-mica and K-feldspar as most abundant inclusions.

Analytical Methods and Sample Preparation

Whole-rock samples

Fresh rock chips of the granitoids were ground in an agate mill and the major element oxides were analyzed on fused glass disks employing a Phillips PW 1500 X-ray fluorescence spectrometer. The precision and accuracy of the major element data as determined on the Chinese whole-rock granite standard GSR-1 (Xie et al., 1985) are ≤5 percent and ca. 5 percent (2σ), respectively (Zhou et al., 2002). The FeO concentrations were determined by titration and the loss on ignition (LOI) gravimetrically. The chemical analyses were carried out at the Institute of Geology and Geophysics of the Chinese Academy of Sciences in Beijing (IGGCAS).

Trace-element abundances were determined by ICP-MS (VG-PQII) at the IGGCAS employing the procedures of Zhou et al. (2002). The sample powders were decomposed in a mixture of distilled HF-HNO_3 in Savillex Teflon® beakers for 6 days at 120°C. The sample solution was dried and the residue dissolved in 50 ml 1 percent HNO_3 for ICP-MS analysis. Indium was used as internal standard for correction of matrix effects and instrumental drift. The procedural blank contribution for the trace elements in Table 2 is ≤446 pg and not significant considering the high concentrations of incompatible elements in the granitoids. The precision and accuracy of the data are better than 5 percent as determined on GSR-1 (Zhou et al., 2002).

Chalcopyrite and biotite samples

Single fragments of chalcopyrite of high quality, weighing 2 to 5 mg, were handpicked from a small (2×3×5 cm) and crushed chalcopyrite specimen under a binocular microscope. In order to minimize the possibility of initial isotopic disequilibrium between individual chalcopyrite grains, the size of chalcopyrite selected for handpicking was kept as small as possible. After washing the chalcopyrite grains in analytical-grade

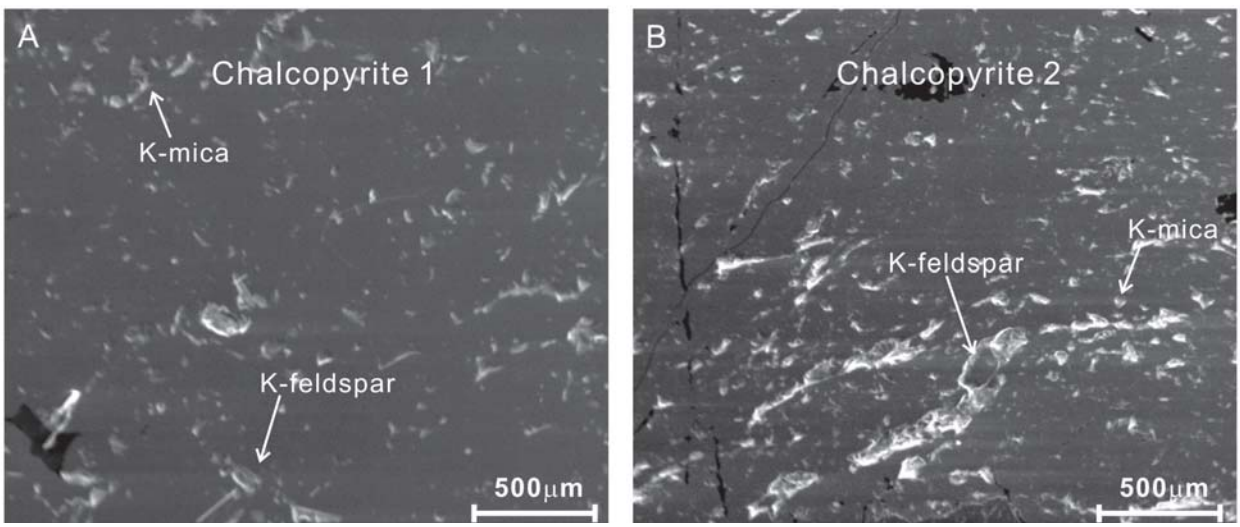

FIG. 3. Scanning electron microscope images of the two varieties of chalcopyrite samples analyzed in this study. (A) Chalcopyrite sample-1 showing isolated mineral inclusions of hydrothermal K-mica and K-feldspar in a dense matrix. (B) Chalcopyrite sample-2 showing K-mica and K-feldspar oriented and concentrated along fractures.

TABLE 1. SEM Analyses of Silicate Mineral Inclusions in Chalcopyrite

	SiO_2 [1]	Al_2O_3	K_2O	MgO	Fe_2O_3	Total	Inferred mineral
Sample-1							
Spot 17	67.13	17.53	11.85	2.41	0.31	99.23	K-feldspar
Spot 25	43.13	37.44	9.73	0.76	2.52	93.58	K-mica
Sample-2							
Spot 48	64.82	18.42	12.36	2.49	0.18	98.25	K-feldspar
Spot 76	48.04	35.56	10.84	1.22	0.54	96.23	K-mica

[1] Concentrations in wt percent

TABLE 2. Major- and Trace-Element Concentrations of the Mo-Cu Hosting Granites

	Syenogranite				Monzogranite			
Sample no.	CG11	CG12	CG13	CG14	CG31	CG32	CG33	CG34
SiO_2	75.09	75.25	74.56	73.96	69.04	70.34	69.30	70.35
TiO_2	0.07	0.06	0.08	0.08	0.24	0.24	0.25	0.25
Al_2O_3	14.32	14.09	13.92	14.83	16.50	15.87	15.91	15.67
Fe_2O_3	0.25	0.44	0.31	0.36	1.13	1.17	2.53	1.37
FeO	0.24	0.32	0.37	0.49	1.03	1.17	0.46	1.09
MnO	0.01	0.04	0.01	0.03	0.03	0.04	0.03	0.05
MgO	0.14	0.15	0.19	0.20	0.58	0.65	0.59	0.69
CaO	0.31	0.53	0.94	1.07	2.90	2.75	2.69	2.91
Na_2O	3.56	4.91	4.09	5.00	4.27	4.20	4.04	4.36
K_2O	5.61	4.03	4.76	3.60	3.58	3.13	3.56	2.37
P_2O_5	0.04	0.03	0.02	0.03	0.09	0.09	0.09	0.09
LOI	0.82	0.62	1.22	0.88	1.08	0.90	1.22	1.36
Total	99.48	99.49	99.49	99.54	99.48	99.56	99.68	99.58
Rb	83.9	77.3	77.6	59.1	54.5	50.3	56.3	48.7
Ba	3550	990	1830	2100	2050	1430	1600	1220
Th	8.74	3.62	4.66	4.15	4.93	6.78	6.75	5.15
U	0.57	0.44	1.25	0.37	0.41	1.58	1.03	0.61
Nb	4.53	9.76	7.40	5.13	4.78	6.13	5.18	5.32
Ta	0.33	0.75	0.37	0.29	0.29	0.39	0.31	0.32
Sr	430	330	470	660	900	730	840	910
Zr	65.3	52.9	57.9	65.7	150	154	153	171
Hf	1.80	1.92	1.73	1.79	3.92	4.15	4.08	4.52
Pb	21.0	18.8	19.8	20.4	16.8	15.2	17.2	15.9
La	27.1	10.5	15.4	17.5	32.7	42.6	44.6	33.5
Ce	56.6	19.7	28.3	30.2	57.8	74.1	76.6	60.0
Pr	4.99	2.16	3.05	3.22	6.12	8.22	8.37	6.33
Nd	15.6	7.7	10.3	10.6	19.7	27.2	26.4	20.3
Sm	2.32	1.63	1.85	1.67	2.95	4.36	4.01	3.04
Eu	0.72	0.52	0.50	0.69	0.95	1.13	1.03	0.89
Gd	1.59	1.37	1.36	1.18	2.04	2.98	2.69	2.02
Tb	0.17	0.22	0.17	0.14	0.22	0.32	0.28	0.20
Dy	0.77	1.24	0.79	0.64	0.85	1.35	1.07	0.78
Y	4.41	7.69	4.90	4.08	5.21	7.35	6.23	4.81
Ho	0.14	0.26	0.15	0.12	0.16	0.24	0.20	0.14
Er	0.44	0.76	0.45	0.40	0.50	0.68	0.61	0.45
Tm	0.08	0.13	0.08	0.07	0.09	0.12	0.11	0.09
Yb	0.58	0.92	0.59	0.52	0.66	0.83	0.74	0.63
Lu	0.09	0.15	0.10	0.09	0.11	0.14	0.12	0.11
La/Yb	47	11	26	34	50	51	60	53
Sr/Y	96	42	95	162	173	100	134	190
Th/U	15.3	8.2	3.7	11.2	12.0	4.3	6.6	8.4
Eu/Eu*	1.15	1.07	0.97	1.50	1.18	0.96	0.96	1.09

Notes: Major elements (wt %) were analyzed by XRF and trace elements (ppm) by ICPMS; LOI = loss on ignition; $Eu/Eu^*=Eu_N/(Sm_N \times Gd_N)^{1/2}$; N = chondrite-normalized concentrations, values from Boynton et al. (1984)

alcohol in an ultrasonic bath and rinsing in ultrapure water, the grains were transferred to Teflon vessels and spiked with a mixed ^{87}Rb-^{84}Sr tracer solution. The samples were dissolved overnight in 0.3 ml 3*N* distilled HNO_3 and 0.1 ml concentrated HF at 80°C.

Single biotite crystals of ca. 0.1 mg were separated from a fresh sample of monzogranite (sample CG 31) under a binocular microscope. They were washed ultrasonically in distilled water and dried before decomposition. The biotite crystals were decomposed by the vapor digestion method in Teflon beakers placed inside a Parr vessel (Li et al., 2008b). Biotite decomposition was achieved at ca. 190°C within 48 hours. The fluorides were converted to nitrates before dissolution of the sample cake in dilute HNO_3.

Separation and purification of Rb and Sr were carried out on Teflon columns filled with ca. 0.1 ml Sr-Spec® resin according to the method of Horwitz et al. (1992). Additional information about these microanalytical procedures is reported in Li et al. (2008a). The Sr fraction was loaded on a W filament with TaF_5 as ion emitter. The isotopic ratios of Rb and Sr were determined on an IsoProbe-T mass spectrometer at IGGCAS. Thermal-mass fractionation of Sr isotopes was corrected with the power law and a $^{86}Sr/^{88}Sr$ ratio of 0.1194. Rb isotope ratios were corrected for thermal-mass fractionation using an empirically determined value of 0.3 percent per a.m.u. In the course of this study, analysis of as little as 200 pg of the NIST-987 Sr reference material yielded $^{87}Sr/^{86}Sr = 0.710250 \pm 31$ (2σ, N = 6). The total procedural blanks for Rb and Sr were 4 ± 1 pg and 6 ± 1 pg (N = 6), respectively. These blank values are about two orders of magnitude lower than those achieved with conventional large column procedures and are not significant for the low-level Rb and Sr samples of this study. The

data-regression analysis for age calculations was performed with ISOPLOT (Ludwig, 2001). The ^{87}Rb decay constant employed is $1.42 \times 10^{-11}a^{-1}$ (Steiger and Jäger, 1977). For the biotite data-regression analysis, we used an error correlation of 0.76 as recommended by Brooks et al. (1972), and input errors are 1.5 percent (2σ) for $^{87}Rb/^{86}Sr$ ratios, 0.01 percent (2σ) for $^{87}Sr/^{86}Sr$ ratios. The same uncertainties were used for the chalcopyrite data-regression analysis.

The separation of Sr, Nd, and Pb from the granite samples followed the procedures of Chen et al. (2007). The isotopic compositions of these elements were measured on a Finnigan MAT-262 mass spectrometer at IGGCAS. Thermal mass fractionation of Sr and Nd isotopes was corrected with a power law and $^{86}Sr/^{88}Sr = 0.1194$ and $^{146}Nd/^{144}Nd = 0.7219$, respectively. Analyses of the NIST-987 reference material yielded $^{87}Sr/^{86}Sr = 0.710253 \pm 0.000010$ (N = 8, 2σ) and for the La Jolla standard $^{143}Nd/^{144}Nd = 0.511862 \pm 0.000009$ (N = 8, 2σ). Five analyses of the reference material NIST-981 yielded $^{206}Pb/^{204}Pb = 16.916 \pm 0.009$ (2σ), $^{207}Pb/^{204}Pb = 15.461 \pm 0.010$ (2σ), $^{208}Pb/^{204}Pb = 36.616 \pm 0.012$ (2σ). The measured Pb isotope ratios were corrected for thermal mass fractionation using a value of 0.1 percent per a.m.u. The total procedure blanks of ca. 1 ng for Sr, Nd, and Pb are not significant for the whole-rock compositions.

Mineral inclusions

The mineral inclusions in chalcopyrite were semiquantitatively analyzed with a Zeiss DSM 960A SEM equipped with an energy dispersive X-ray analysis system at the Department of Earth and Environmental Sciences, Universität München.

Results

Rb-Sr mineral chronology

The Rb-Sr isotope data of the chalcopyrite samples and biotite crystals are listed in Table 3 and plotted in isochron diagrams in Fig. 4. The Rb and Sr concentrations in the chalcopyrite grains show very large differences resulting in Rb/Sr ratios varying by a factor of over 300. The Rb concentrations are overall low and vary by a factor of 350 from 0.01 to 3.5 ppm; Sr concentrations range from 3.4 to 38 ppm. These lithophile element concentrations reflect primarily the abundance and composition of K-mica and K-feldspar inclusions and possibly subordinate, but not optically observed in this study, fluid inclusions in the chalcopyrite which typically does not incorporate lithophile elements in its lattice. All seven grains analyzed of chalcopyrite sample-1 (i.e., the sample showing no obvious deformation features) yielded a data trend with a slope that corresponds to an age of 255 ± 37 Ma (2σ, Fig. 4A) Two data points plot off the common, well-defined data trend so that the regression analysis yields a high MSWD of 31. We suggest that these two chalcopyrite fragments either preserved initial isotopic heterogeneity among silicate minerals or contain isotopically heterogeneous fluid inclusions. Excluding these two analyses (chalcopyrite samples F2 and F6, Table 3, Fig. 4A), the data regression analysis yields a nearly identical but more precise isochron age of 256 ± 6 Ma (2σ, MSWD = 0.3).

The ^{87}Rb decay constant ($\lambda\ ^{87}Rb$) we have used is $1.42 \times 10^{-11}a^{-1}$ (Steiger and Jäger, 1977), and it has ca. 1.5 percent uncertainty as suggested by, for example, Minster et al. (1982). Including this uncertainty the Rb-Sr isochron age is 256 ± 7 Ma (2σ). A Re-Os age of 258 ± 3 Ma (2σ, $\lambda\ ^{187}Re = 1.666 \times 10^{-11}a^{-1}$) for a molybdenite sample from the same deposit was obtained by J. Liu (pers. commun., 2007). Taking an uncertainty of $\lambda\ ^{187}Re$ of 1.02 percent into account (Smoliar et al., 1996), the Re-Os isochron age becomes 258 ± 4 Ma (2σ). Thus, including the uncertainties of the decay constants does not change the fact that our chalcopyrite Rb-Sr age is, within error limits, indistinguishable from the Re-Os age. The good agreement of the Rb-Sr and Re-Os ages lends strong support to the assumption that the Rb-Sr isotopic system in small-grain chalcopyrite samples can be used to determine meaningful ages for chalcopyrite crystallization.

Seven chalcopyrite grains separated from a second, slightly deformed—that is, fractured—specimen (sample-2, Table 3) collected only a few meters away from chalcopyrite sample-1 yielded a much younger age of 207 ± 15 Ma (2σ, MSWD = 14, Fig. 4B). Actually we also realized that rejection of two points would improve the age uncertainty. Doing so yields 205 ±12 Ma (2σ, MSWD = 4), which is very similar to the result of the seven-point data regression, although the uncertainty has been reduced. However, we preferred the larger age uncertainty as reasonable because the chalcopyrite sample 2 represented a prolonged open system as can be inferred from Figure 3, showing fractures and linearly oriented and connected mineral inclusions. The much younger age and high MSWD value for the fractured chalcopyrite sample support an open-system behavior of the Rb-Sr system as discussed below.

TABLE 3. Rb- and Sr Isotope Compositions of Single-Grain Chalcopyrite and Biotite Samples

	Rb (ppm)	Sr (ppm)	$^{87}Rb/^{86}Sr$	$^{87}Sr/^{86}Sr$	$2\sigma_m$
Chalcopyrite sample-1					
F1	0.121	5.32	0.0656	0.709550	12
F2	0.306	4.84	0.183	0.710328	11
F3	0.843	3.39	0.719	0.711940	10
F4	0.964	24.4	0.114	0.709745	11
F5	0.717	7.79	0.266	0.710276	23
F6	0.011	12.0	0.0026	0.709123	16
F7	0.657	15.2	0.125	0.709800	14
Chalcopyrite sample-2					
F1	1.02	18.8	0.156	0.709929	9
F2	0.078	6.52	0.035	0.709698	10
F3	1.34	7.20	0.537	0.711020	13
F4	3.46	9.65	1.04	0.712456	14
F5	0.131	37.8	0.0100	0.709247	10
F6	1.58	4.76	0.957	0.712284	12
F7	0.187	3.72	0.145	0.709845	11
Biotite samples of monzogranite CG 31					
C1	70.3	3.93	52.7	0.896462	63
C2	67.5	2.31	87.1	1.014729	20
C3	145	8.41	50.6	0.889433	25
C4	103	4.49	67.7	0.945350	45
C5	164	9.98	48.2	0.878408	22
C6	64.6	5.72	33.0	0.826950	58
C7	84.7	3.29	76.5	0.977880	30

Notes: F1 to F7 represent individual fragments of chalcopyrite; C1 to C7 represent single biotite crystals; the $2\sigma_m$ error refers to the last digits

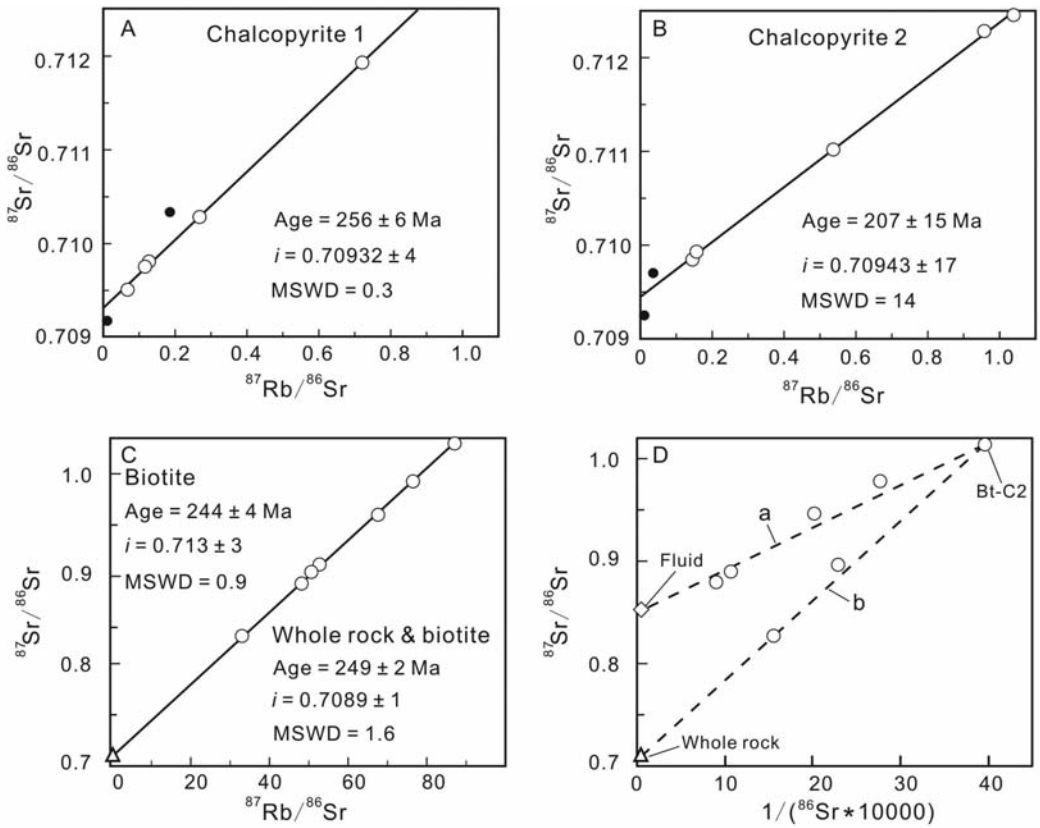

FIG. 4. Rb-Sr isochron diagrams for the two texturally different chalcopyrite samples 1 (A) and 2 (B), and single biotite crystals from monzogranite sample CG 31 (C) The two solid data points in Figure 4A were rejected for age calculations (see text). Note that the rejection of data points does not change the age but reduces the error. (D) $^{87}Sr/^{86}Sr$ vs. $1/^{86}Sr$ diagram for biotite crystals and whole-rock monzogranite sample CG 31 revealing mixing trends. The upper data trend (a) suggests isotopic equilibration of biotite with a Sr-rich hydrothermal fluid during cooling. The composition of the fluid is inferred. The lower data trend (b) can be explained with presence of mineral inclusions (K-feldspar?) in biotite. Apparently, the mixing trends have age significance; see Discussion.

The Rb-Sr data of seven single biotite crystals and the whole-rock sample of hosting monzogranite CG 31 yielded an apparent age of 249 ± 2 Ma (2σ, MSWD = 1.6, Fig. 4C). The initial $^{87}Sr/^{86}Sr$ ratio of 0.7089 is similar to that of the mineral inclusions in the chalcopyrite samples. A similar isochron age of 244 ± 4 Ma (2σ, MSWD = 0.9) for the seven biotite data points alone (i.e., without the whole-rock data) corroborates our interpretation of the whole-rock biotite age as the time of cooling of the granite below ca. 300° to 400°C (see review of Willigers et al., 2004). A plot of $^{87}Sr/^{86}Sr$ vs. 1/Sr reveals for the whole-rock and biotite data two trends with biotite sample fraction C2 as a common endmember (Fig. 4D). The samples plotting along the trend "b," including the whole-rock sample, yielded an age of 250 ± 2 Ma (2σ, MSWD = 1.7, initial $^{87}Sr/^{86}Sr$ = 0.70890 ± 6). The data trend "a" is based on biotite analyses alone and the samples plotting along this trend yielded an age of 244 ± 7 Ma (2σ, MSWD = 1.2, initial $^{87}Sr/^{86}Sr$ = 0.713 ± 6), which is indistinguishable within error limits from the 250 Ma whole-rock–biotite age and the 249 ± 2 Ma cooling age based on all data points.

Major- and trace-element data of the Mo-Cu hosting granites

The chemical compositions of the ore-hosting granites at Chehugou mine are listed in Table 2 and plotted in Figs. 5 and 6. The normative quartz and feldspar proportions derived from the CIPW-norm show a spectrum of rock types including monzogranite and more alkalic syenogranite. These rock compositions suggest rifting environments in orogens, collisional to post-collisional settings, rather than arc-settings (Fig. 5A). The SiO_2 concentrations of ca. 69 to 75 wt percent indicate highly evolved rock compositions distinct from typical intermediate subduction-related igneous rocks. According to the molar ratios of Al/Ca, Na, and K, the granites have transitional I- to S-type affinities with a sedimentary component reflected in their peraluminous composition (Fig. 5B).

The granites show high La/Yb ratios up to 60, high Sr/Y ratios up to 190 and low Yb concentrations <0.9 ppm. These data together with the REE pattern (Fig. 6, discussed below) indicate garnet and amphibole as residual phases during partial melting or as liquidus phases during fractional magma crystallization. The features were originally interpreted as due to melting of subducted oceanic crust (Defant and Drummond, 1990), but there is increasing evidence that melting of lower crust can also explain such trace-element characteristics (Rapp et al., 1999; Xu et al., 2002; Gao et al., 2004). For the granites of this study, the radiogenic isotopes indicate melting of old and lower continental crust.

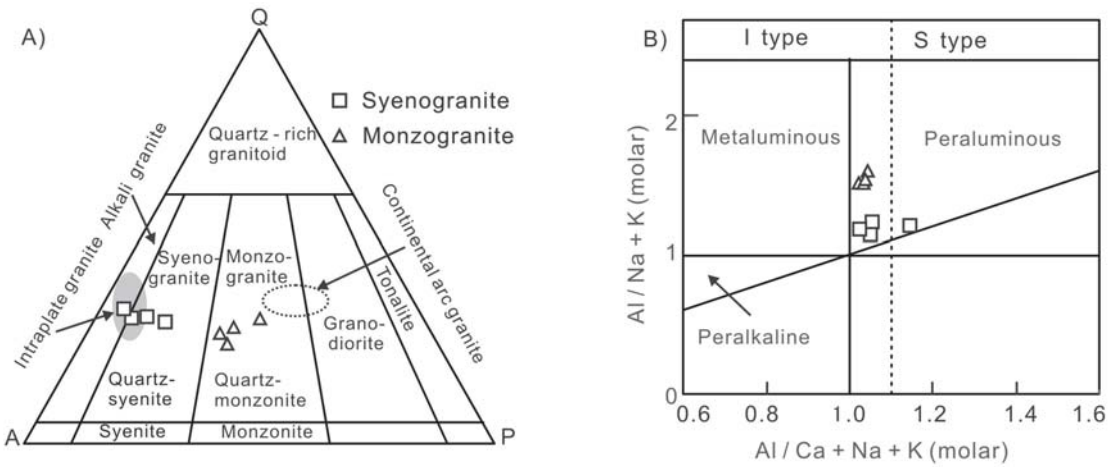

FIG. 5. Major-element characteristics of the Mo-Cu hosting granites from the Chehugou mine. (A) QAP diagram (Streckeisen, 1976) showing rock types according to their normative mineral proportions. The granites of this study show arc to intraplate affinities. Fields for intraplate granites from Wu et al. (2002) and continental arc granites from Chen et al. (2000). (B) Molar ratios of Al/Ca, Na, K (Shand, 1943) in samples of this study revealing transitional I- to S-type compositions. The stippled line delineates I-type from S-type granite.

The normalized trace-element patterns are indistinguishable for the syenogranite and monzogranite samples (Fig. 6). All samples show a crustal signature including a positive Pb and negative Nb anomalies and enrichment of Sr relative to Nd and Pr. The HREE patterns in most samples are concave, suggesting fractionation and/or residual amphibole with high distribution coefficients for the intermediate HREE (Bottazzi et al., 1999). Eu/Eu* ratios of 0.96 to 1.5 indicate absence of or slightly positive Eu anomalies in the samples, consistent with melt evolution in the deep crust and minor accumulation of feldspar.

Sr, Nd, and Pb isotope compositions of the granites

The Sr-Nd isotope compositions of granites are listed in the Table 4 and plotted in Fig. 7. Initial ratios were calculated for an inferred age of 260 Ma. The monzogranite samples have initial $^{87}Sr/^{86}Sr$ ratios of ca. 0.7087 to 0.7089 and uniform $\varepsilon_{Nd(t)}$ values of –20.6 to –20.8. The syenogranites have slightly

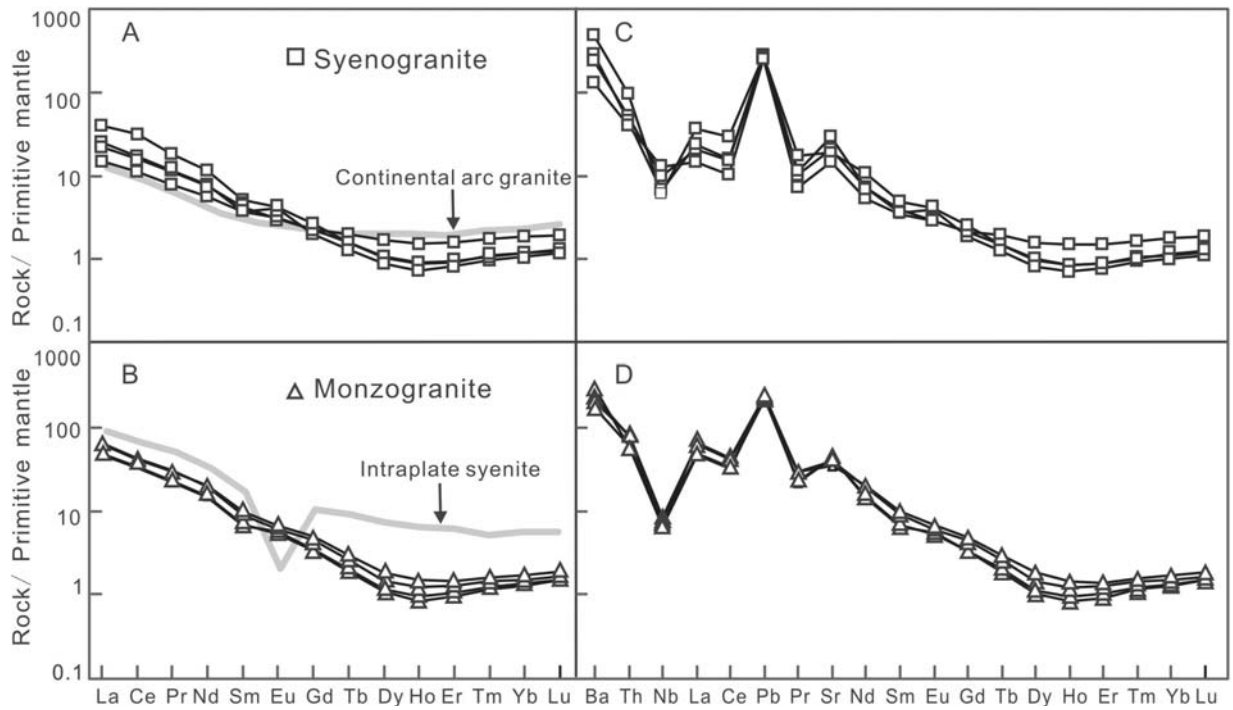

FIG. 6. Primitive mantle-normalized trace-element patterns for syenogranite (A, C) and monzogranite samples (B, D). Normalizing data from Sun and McDonough (1989). Patterns shown for comparison include typical intraplate syenite and magmatic arc granodiorite (Liu et al., 2005; Yang et al., 2008).

TABLE 4. Sr- and Nd Isotope Compositions of the Mo-Cu Hosting Granites

Sample no.	Rb (ppm)	Sr (ppm)	$^{87}Rb/^{86}Sr$	$^{87}Sr/^{86}Sr \pm 2\sigma_m$	$^{87}Sr/^{86}Sr_{(t)}$	Sm (ppm)	Nd (ppm)	$^{147}Sm/^{144}Nd$	$^{143}Nd/^{144}Nd \pm 2\sigma_m$	$\varepsilon_{Nd(t)}$	t_{DM} (Ga)
Syenogranite											
CG 11	81.8	430	0.552	0.712936 ± 12	0.71089	2.068	15.39	0.0813	0.511269 ± 10	–22.9	2.0
CG 12	72.8	317	0.665	0.714534 ± 8	0.71208	1.277	6.496	0.1189	0.511354 ± 12	–22.5	2.7
CG 13	111	455	0.707	0.711576 ± 14	0.70896	1.547	9.231	0.1014	0.511333 ± 12	–22.3	2.3
CG 14	55.6	662	0.243	0.711658 ± 15	0.71076	1.474	10.07	0.0886	0.511288 ± 09	–22.8	2.1
Monzogranite											
CG 31	58.5	932	0.182	0.709540 ± 9	0.70887	2.823	20.40	0.0836	0.511382 ± 12	–20.8	2.0
CG 32	52.8	778	0.196	0.709413 ± 14	0.70869	4.097	27.97	0.0886	0.511399 ± 10	–20.6	2.0
CG 33	55.8	850	0.190	0.709533 ± 13	0.70883	3.482	25.34	0.0831	0.511388 ± 11	–20.6	1.9
CG 34	45.9	963	0.138	0.709364 ± 13	0.70885	2.814	20.77	0.0819	0.511375 ± 14	–20.8	1.9

Notes: Initial $^{87}Sr/^{86}Sr_{(t)}$ and $\varepsilon_{Nd\,(t)}$ were calculated for an age of 260 Ma; reference values: $^{143}Nd/^{144}Nd_{CHUR(0)} = 0.512638$, $^{147}Sm/^{144}Nd_{\,CHUR(0)} = 0.1967$, $\lambda^{87}Rb = 1.42\times10^{-11}a^{-1}$, $\lambda^{147}Sm = 6.54\times10^{-12}a^{-1}$; t_{DM} calculated according to DePaolo (1981); the $2\sigma_m$ error refers to the last digits

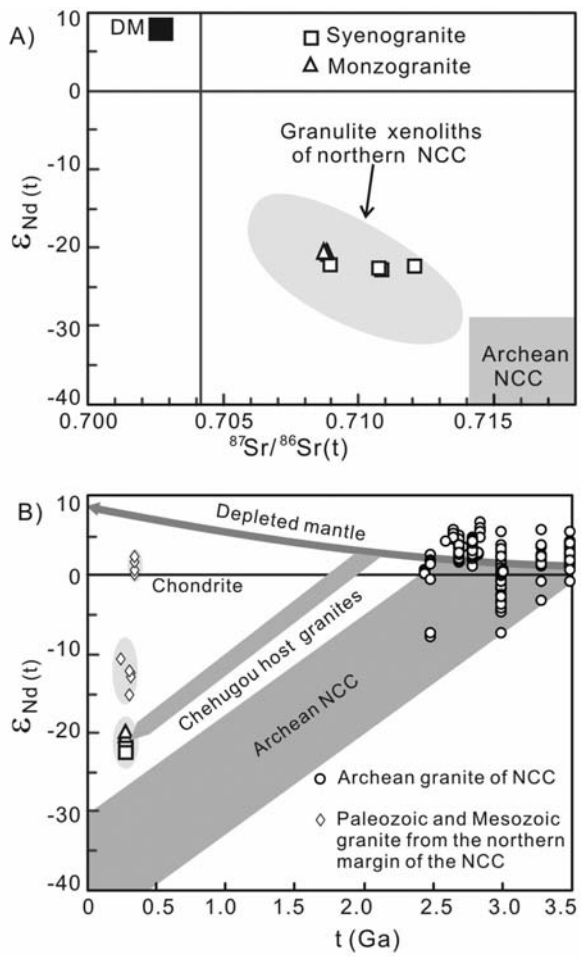

FIG. 7. (A) Initial Sr-Nd isotope data of granites from Chehugou Mo-Cu deposit assuming an age of 260 Ma. The data indicate old lower crustal sources as sampled by granulite-facies xenoliths from the Archean North China craton (NCC). The shaded field outlines the xenolith data recalculated to 260 Ma. Data sources: DM (depleted mantle) from Salters and Stracke (2004); Granulite xenolith data from Zhou et al. (2002), Zheng et al. (2004), Jiang et al. (2007); North China craton data from Wu et al. (2005) (B) ε_{Nd} values in samples of this study compared with those for granites from the Archean North China craton (data compilation in Wu et al., 2005) and Paleozoic-Mesozoic granite (data from Chen et al., 2000; Jiang et al., 2007; and Liu et al., 2005).

more enriched isotopic signatures and suggest crustal sources, as indicated by initial $^{87}Sr/^{86}Sr$ ratios of ca. 0.7090 to 0.7121 and uniform $\varepsilon_{Nd\,(t)}$ values of –22.3 to –22.9. The average crustal residence time of the source material of the granites is 1.9 to 2.2 Ga (Fig. 7; DePaolo, 1981). The initial Nd isotope ratios of the granitoids plot above the isotope evolution trend of typical Archean North China craton, consistent with crustal sources comprising a small amount of a juvenile mantle-derived component. There is good agreement with the composition of lower crustal granulite-facies xenoliths sampled by ca. 140 Ma old volcanism (see references in Fig. 7).

The Pb isotope compositions of the samples are listed in the Table 5 and plotted in Fig. 8. Syeno- and monzogranite samples have indistinguishable Pb compositions, dominated by a Neoproterozoic crustal component (Zartman and Doe, 1981). The high $^{208}Pb/^{204}Pb$ ratios relative to $^{206}Pb/^{204}Pb$ indicate crustal sources with a long-term evolution with a high Th/U ratio probably due to loss of U as has been suggested for granulite-facies metamorphism of the lower crust (e.g., DePaolo et al., 1982; Rudnick et al., 1985). The corresponding $^{207}Pb/^{204}Pb$ ratios are higher than the model lower crustal composition and indicate the presence of material that evolved with a high $^{235}U/^{204}Pb$ ratio, as can be assumed for Archean upper crust. A subordinate juvenile mantle-derived component as suggested by Nd isotopes will not be obvious in the Pb isotopes, as the Pb isotopes in the samples will be reflect the crustal components owing to the much higher Pb concentration in crust than in a mantle-derived basalt.

Discussion

Ages of the Mo-Cu mineralization and hosting granites

The Rb-Sr isotope data for minute single fragments of chalcopyrite separated from a massive hand specimen (chalcopyrite sample 1) provide a robust isochron age of 256 ± 7 Ma (2σ, including λ uncertainty, MSWD = 0.3). The excellent agreement of this datum with that derived from a 7-data point errorchron of 255 ± 37 Ma as well as an Re-Os age of 258 ± 3 Ma for molybdenite from the same mine (J. Liu, pers. commun., 2007) corroborates the geologic significance of the Rb-Sr chalcopyrite age of this study.

TABLE 5. Pb Isotope Compositions of the Mo-Cu Hosting Granites

Sample no.	$^{206}Pb/^{204}Pb_{m.}$	$^{207}Pb/^{204}Pb_{m.}$	$^{208}Pb/^{204}Pb_{m.}$	$^{238}U/^{204}Pb$	$^{235}U/^{204}Pb$	$^{232}Th/^{204}Pb$	$^{206}Pb/^{204}Pb_{t}$	$^{207}Pb/^{204}Pb_{t}$	$^{208}Pb/^{204}Pb_{t}$
Syenogranite									
CG11	16.704 ± 7	15.368 ± 7	37.777 ±6	1.91	0.014	29.5	16.62	15.36	37.40
CG12	16.650 ± 8	15.434 ± 9	37.967 ±8	1.65	0.012	13.7	16.58	15.43	37.79
CG13	16.868 ± 8	15.412 ± 8	37.915 ±8	4.46	0.032	16.8	16.68	15.40	37.70
CG14	16.592 ± 6	15.385 ± 6	37.621 ±7	1.27	0.0092	14.4	16.54	15.38	37.44
Monzogranite									
CG31	16.578 ± 7	15.418 ± 9	38.167 ±8	1.73	0.012	20.9	16.51	15.41	37.90
CG32	16.992 ± 7	15.411 ± 8	37.762 ±8	7.35	0.053	31.7	16.69	15.40	37.35
CG33	16.857 ± 9	15.406 ± 9	37.751 ±9	4.23	0.031	27.9	16.68	15.39	37.39
CG34	16.635 ± 8	15.391 ± 9	37.712 ±9	2.70	0.020	22.9	16.52	15.39	37.42

Notes: m.= measured ratios, t = initial ratios for an age of 260 Ma; errors are $2\sigma_m$ and refer to the last digits; U, Th/Pb isotope ratios calculated with concentration data of Table 1

As outlined above, the chalcopyrite age is, strictly speaking, the time of incorporation into the chalcopyrite grain and diffusive isolation of isotopically similar or equilibrated hydrothermal silicate minerals, in this case predominantly K-mica and K-feldspar, by chalcopyrite precipitation from Mo-Cu rich hydrothermal fluids, in a slowly cooling granite body. The fact that the data plot along a nearly perfect isochron implies that (1) the enclosed hydrothermal mineral phases in each chalcopyrite fragment had, at time of isolation, an identical isotopic composition and (2) that the silicate minerals became thereafter isolated (closed-system isotopic evolution) to evolve to their present isotope composition. The first implication reflects the open-system behavior of the whole-rock sample during hydrothermal activity, allowing for isotopic exchange both between the different silicate phases and between silicates and fluid. The second implication indicates that the open-system conditions were terminated due to sealing of the inclusions by the crystallizing chalcopyrite. Therefore, the calculated age refers to the crystallization of the chalcopyrite and thus to the mineralization process itself.

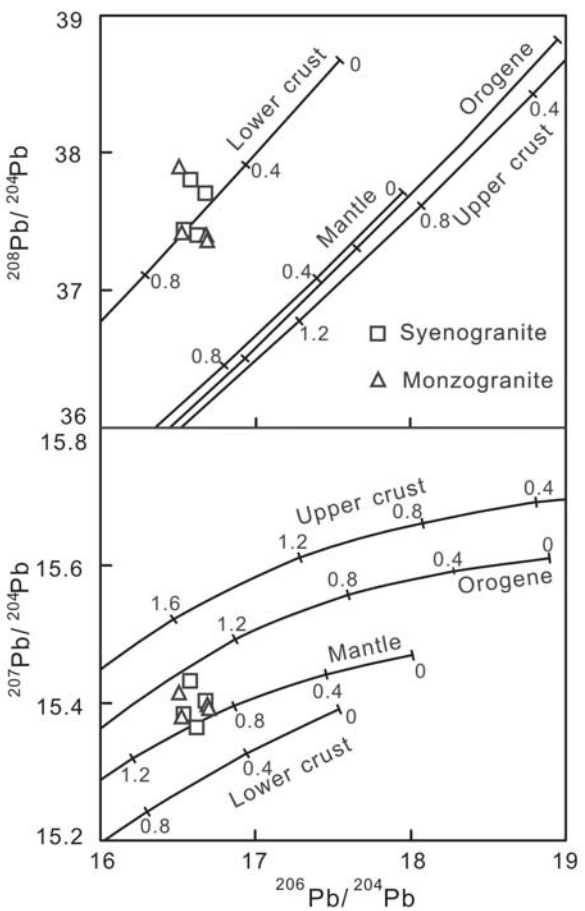

FIG. 8. Initial Pb isotope compositions of the Chehugou granites. Shown are model isotopic evolution curves for Pb in mantle and crustal reservoirs (Zartman and Doe, 1981). The ticks on the curves indicate age intervals in Ga. High $^{208}Pb/^{204}Pb$ ratios relative to the $^{206}Pb/^{204}Pb$ ratios indicate crustal sources with a long-term evolution with a high Th/U ratio as inferred for granulite-facies lower crust (e.g., DePaolo et al., 1982; Rudnick et al., 1985). $^{207}Pb/^{204}Pb$ ratios plotting above the lower crust curve consistent with presence of subordinate amounts of ancient upper crustal material in the inferred lower crustal granite source.

Both the agreement of the Rb-Sr chalcopyrite age with the Re-Os molybdenite age and the isochron relationship for five out of seven chalcopyrite fragments further support our assumption that the chalcopyrite grains had reached a high degree of initial isotopic homogeneity and evolved thereafter in a closed system, all prerequisites for a reliable age determination. This prerequisite for a meaningful age determination can be accomplished by isotopic exchange among the hydrothermal minerals in contact with hot 800° to 350°C (Barton, 2000; Seedorff et al., 2005) Mo-Cu rich hydrothermal fluids. The observation that the sample grains of chalcopyrite-1 are characterized by a dense, nonfractured matrix and interspersed isolated hydrothermal mineral inclusions is good evidence to propose 256 Ma as the mean age of the formation of chalcopyrite mineralization. Taking into account that the geochemically very different Re-Os system in molybdenite (crystallization temperature >440°C, Selby and Creaser, 2001) yielded, within error limits, an identical age of 258 ± 3 Ma strengthens our conclusion that the Rb-Sr chalcopyrite age does, indeed, reflect the ore-forming process. Thus, we propose that the Rb-Sr system in chalcopyrite grains from small isotopically equilibrated samples is an additional geologic chronometer to constrain the time of Mo-Cu mineralizations. In order to bracket the entire duration of the Mo-Cu mineralization in the Chehugou mining district, additional age determinations with both the Rb-Sr and Re-Os and, especially, the U-Pb-zircon chronometers are required. With the data at hand we suggest ca. 256 Ma as the mean age of

major Mo-Cu mineralization at the Chehugou mine and an extended time span of ca. 250 to 260 Ma when including the errors of the different methods and associated errors. This finding strongly indicates that the Mo-Cu mineralization is related to the closure of the Paleo-Asian Ocean rather that the Yanshanian orogeny lasting from 160 to 60 Ma, as previously had been assumed (BGMRIM, 1991).

The surprisingly young age of ca. 207 Ma for chalcopyrite sample-2 is interpreted as related to rock deformation during crystallization of the chalcopyrite and prolonged diffusion of Rb and Sr along grain boundaries and fractures. The evidence for fractures and linearly oriented and connected mineral inclusions in SEM photos (Fig. 3) underlines the assumption that the chalcopyrite sample was prone to open-system behavior and isotopic reequilibration among the hydrothermal minerals by circulating fluids. Indeed, it has been shown that elemental diffusion at grain boundaries and cracks is efficient at temperatures much lower than assumed for intracrystalline volume diffusion (Kaur et al., 1995), and we suggest that at ca. 207 Ma, hydrothermal activity and fluid circulation had ceased at Chehugou and/or that temperatures were too low to for diffusive exchange. This finding leads to the economically important conclusion that the Yanshanian orogeny had no major tectonothermal effect on the rocks in the Chehugou region.

Regarding the magmatic age of the Mo-Cu–hosting granites, the Rb-Sr chalcopyrite and Re-Os molybdenite ages of ca. 250 to 260 Ma provide good evidence that emplacement of the hosting granites occurred not much earlier than ca. 260 Ma. The biotite data suggest that the granite cooled below 300° to 400°C (see review of data in Willigers et al., 2004), at ca. 249 Ma, about 10 m.y. after crystallization of molybdenite and chalcopyrite. The biotite cooling age of 249 Ma can also be interpreted as a lower age limit for the Mo-Cu mineralization.

We assessed whether or not two-component mixing can explain the linear alignment of data points (Faure, 1986; Fig. 4D). The trend "b" may be explained by the presence of other whole-rock components (e.g., magmatic inclusions, such as feldspar) in the two biotite samples with intermediate composition, whereas biotite sample C2 may present a pure end-member composition. The age of 250 ± 2 Ma derived from this trend is meaningful with respect to cooling of the granite. The data trend "a" is based on biotite analyses alone and we prefer to explain it by variable overprinting of biotite grains such as C2 with a Sr-rich hydrothermal fluid isotopically not much different from the whole rock. Variable degrees of biotite overprinting by a fluid can be concluded as all data points are well correlated. The age of 244 ± 7 Ma derived from trend "a" is indistinguishable within error limits from the 250 Ma whole rock-biotite age (trend "b") and the 249 ± 2 Ma cooling age based on all data points. This underlines the fact that all mixing components and mixtures were isotopically identical or similar at the time of closure of the Rb-Sr system, and that the mixing trends discussed above must have age significance with respect to cooling of the granite below the closure temperature of biotite at ca. 250 Ma.

Sources of the Mo-Cu host granites and mineralizing fluids

The Chehugou ore deposit is a typical porphyry-type deposit and constraints on its origin will shed light on the nature of the Mo-Cu–bearing hydrothermal fluids in general. Although both types of host granites were derived from similar lower crustal sources as indicated by Sr, Nd, and Pb isotopes, the economically important mineralization is confined to the chemically more evolved syenogranite rather than the less evolved monzogranite. The major element data in Table 2 show that the syenogranite represents a highly differentiated residual granitoid magma, whereas the almost barren monzogranite is chemically much less fractionated. This relationship suggests that major Mo-Cu mineralization in the Chehugou region resulted from the enrichment of Mo and Cu in a fluid phase separating from a granitic melt in the course of extensive crystal magma fractionation.

The overall agreement between the initial $^{87}Sr/^{86}Sr$ ratio of 0.7093 in the chalcopyrite samples and a mean initial $^{87}Sr/^{86}Sr$ ratio of 0.7097 in the granites strongly supports derivation of the Mo-Cu hydrothermal fluids from ultimately the same crustal source. The Nd isotope data indicate melting of predominantly Archean crustal sources with a mean residence time of ca. 2 Ga, probably including a minor juvenile mantle-derived component. The high $^{208}Pb/^{204}Pb$ ratios are consistent with lower crustal sources that underwent granulite-facies metamorphism and concomitant U-loss and elevation of Th/U long before crustal melting. Elevated initial $^{207}Pb/^{204}Pb$ ratios indicate additional presence of an Archean upper crustal component that evolved with a high $^{235}U/^{204}Pb$ ratio. As strongly supported by the similar Sr-Nd isotopes in granulite xenoliths from the northern North China craton and the granitoids of this study (Fig. 7), partly rejuvenated lower Archean crust has also been sampled by the ca. 140 m.y. old volcanism at the northern North China craton (Fig. 7; Zhou et al., 2002; Zheng et al., 2004; Jiang et al., 2007). During the Paleozoic-Mesozoic, the northern North China craton constituted an Andean-type continental margin (Wu et al., 2002) undergoing melting and rejuvenation by input of juvenile mantle-derived material. Lower crustal melting and formation of granitoids at ca. 260 Ma was probably also facilitated by input of juvenile mantle-derived magmas, although the isotope data of the granitoids indicate melting of predominantly Archean crust.

Implications for the closure of the Paleo-Asian Ocean

The evidence for a predominantly lower crustal origin of the Mo-Cu-bearing granites at the Chehugou mine may add to the discussion of evidence about the temporal framework of the closure of the Paleo-Asian Ocean. In light of the evidence for melting of predominantly older continental crust, we suggest that lithospheric delamination may be the reason for underplating and melting of the lower crust by hot basaltic magmas (Hanson and Kroner, 1981; Herzberg et al., 1983; Atherton and Petford, 1993). Dehydration melting of mafic lower crust can account for the transitional arc to intraplate affinity of the granitoids with compositions that agree with felsic magmas produced by dehydration melting of lower crustal compositions (Rapp et al., 1999). Extensive mantle melting and crustal magma underplating in orogenic belts leads to overthickened crust (Bird, 1978; Houseman et al., 1981; Nelson, 1992) prone to delamination. The crust at northern margin of the craton must have been overthickened because it constituted an active continental margin since

Silurian (Coleman, 1994; Davis et al., 2001; Johnson et al., 2001; Xiao et al., 2003). Crustal thinning, a typical consequence of lithospheric delamination (e.g., Bird, 1978) has been invoked for the North China craton during the Mesozoic (Griffin et al., 1998; Xu et al., 2002; Gao et al., 2004; Wu et al., 2005). Gao et al. (2004) interpreted the granulite xenolith data as evidence for delamination under the northeastern margin of the craton before 140 Ma. Considering the evidence for melting of lower crustal sources in the Chehugou region, we suggest a late orogenic to postcollision setting with lithospheric delamination at ca. 260 Ma and closure of the Paleo-Asian Ocean in this region in the late Permian.

Conclusions

Rb and Sr isotopes in small fragments of chalcopyrite document for the first time the suitability of the Rb-Sr method for constraining the time of chalcopyrite crystallization. Rb-Sr chalcopyrite ages constrain the mineralization at the Chehugou porphyry Mo-Cu deposit at ca. 256 Ma, indicating that the deposit predates processes related to the Yanshanian orogeny. Rb-Sr biotite ages for a monzogranite sample indicate cooling below ca. 300° to 400°C at ca. 250 Ma, interpreted as a lower age limit for the Mo-Cu mineralization. The emplacement age of the Mo-Cu hosting granitoids is probably not much older than ca. 260 Ma, as can be inferred from the age spectrum of the associated ore minerals.

The radiogenic isotope characteristics of the granites indicate a principal origin from Archean lower crust. Lithospheric delamination may have facilitated crustal melting in late orogenic to postcollision phase. Closure of the Paleo-Asian Ocean north of the Chifeng area may have occurred before 260 Ma, possibly during the middle Permian.

Acknowledgments

This work was supported by National Basic Research Program of China (Grant 2006CB403506, to L. Zhang). B. Wan thanks X. Li and P. Xiao for help with the mass spectrometric measurements and F. Söllner for instructions on the SEM. The paper was written during a visit of B. Wan to Munich University financed by the LMU-China Scholarship Council Program. Reviews by Bruce Eglington and an anonymous reviewer helped to improve this manuscript.

July 9, 2008; March 20, 2009

REFERENCES

Ashleman, J.C., Taylor, C.D., and Smith, P.R., 1997, Porphyry molybdenum deposits of Alaska, with emphasis on geology of Quartz Hill deposit, southeastern Alaska; Economic Geology Monograph 9, p. 334–354.

Atherton, M.P., and Petford, N., 1993, Generation of sodium-rich magmas from newly underplated basaltic crust: Nature, v. 362, p. 144–146.

Barton, M.D., 2000, Overview of the lithophile-element-bearing magmatic hydrothermal system at Birch Creek, White Mountains, California: Society of Economic Geologists Guidebook Series, v. 32, p. 9–26.

Bird, P., 1978, Initiation of intracontinental subduction in Himalaya: Journal of Geophysical Research, v. 83, p. 4975–4987.

Bottazzi, P., Tiepolo, M., Vannucci, R., Zanetti, A., Brumm, R., Foley, S.F., and Oberti, R., 1999, Distinct site preferences for heavy and light REE in amphibole and the prediction of Amph/LDREE: Contributions to Mineralogy and Petrology, v. 137, p. 36–45.

Boynton, W.V., 1984, Geochemistry of the rare earth elements: Meteorite studies, *in* Henderson, P., eds., Rare earth element geochemistry: Amsterdam, Elsevier, p. 63–114.

Brooks, C., Hart, S.R., and Wendt, I., 1972, Realistic use of two-error regression treatments as applied to rubidium-strontium data: Reviews of Geophysics and Space Physics, v. 10, p. 551–577.

Bureau of Geology and Mineral Resources of Inner Mongolia (BGMRIM), 1991, Regional Geology of Nei Mongol (Inner Mongolia) Autonomous Region: Beijing, Geological Publishing House, 775 p. (in Chinese).

Chen, B., Jahn, B.M., Wilde, S., and Xu, B., 2000, Two contrasting paleozoic magmatic belts in northern Inner Mongolia, China: Petrogenesis and tectonic implications: Tectonophysics, v. 328, p. 157–182.

Chen, F., Li, X., Wang, X., Li, Q., and Siebe, W., 2007, Zircon age and Nd-Hf isotopic composition of the Yunnan Tethyan belt, southwestern China: International Journal of Earth Sciences, v. 96, p. 1179–1194.

Chen, Z., Mao, D., Zuo, Y., Li, H., Zhang, C., and Xiang, H., 2003, Mesozoic intrusive magmatism related metallogenetic system in Beichagoumen area: Acta Geoscientica Sinica, v. 25, p. 224–228 (in Chinese with English abs.).

Christensen, J.N., Halliday, A.N., Leigh, K.E., Randell, R.N., and Kesler, S.E., 1995, Direct dating of sulfides by Rb-Sr: A critical test using the Polaris Mississippi Valley-type Zn-Pb deposit: Geochimica et Cosmochimica Acta, v. 59, p. 5191–5197.

Coleman, R.G., 1994, Reconstruction of the Paleo-Asian Ocean: Proceedings of the 29th International Geological Congress, Part B, Utrecht, VSP International Science Publishers, 186 p.

Davis, G.A., Zheng, Y., Wang, C., Darby, B.J., Zhang, C., and Gehrels, G., 2001, Mesozoic tectonic evolution of the Yanshan fold and thrust belt, with emphasis on Hebei and Liaoning Provinces, Northern China, *in* Hendrix, M.S., and Davis, G.A., eds., Paleozoic and Mesozoic tectonic evolution of central and eastern Asia. Memoir 194: Colorado, Geological Society of America, p. 171–197.

Defant, M.J., and Drummond, M.S., 1990, Derivation of some modern arc magmas by melting of young subducted lithosphere: Nature, v. 347, p. 662–665.

DePaolo, D.J., 1981, Neodymium isotopes in the Colorado Front Range and crust-mantle evolution in the Proterozoic: Nature, v. 291, p. 193–196.

DePaolo, D.J., Manton, W.I., Grew, E.S., and Halpern, M., 1982, Sm-Nd, Rb-Sr and U-Th-Pb systematics of granulite facies rocks from Fyfe Hills, Enderby Land, Antarctica: Nature, v. 298, p. 614–618.

Dobretsov, N.L., Berzin, N.A., and Buslov, M.M., 1995, Opening and tectonic evolution of the Paleo-Asian Ocean: International Geology Review, v. 37, p. 335–360.

Faure, G., 1986, Principles of isotope geology: New York, John Wiley, 589 p.

Gao, S., Rudnick, R.L., Yuan, H.L., Liu, X.M., Liu, Y.S., Xu, W.L., Ling, W.L., Ayers, J., Wang, X.C., and Wang, Q.H., 2004, Recycling lower continental crust in the North China craton: Nature, v. 432, p. 892–897.

Griffin, W.L., Zhang, A., O'Reilly, S.Y., and Ryan, C.G., 1998, Phanerozoic evolution of the lithosphere beneath the Sino-Korean craton, *in* Flower, M., Chung, S.L., Lo, C.H. and Lee, T.Y., eds., Mantle Dynamics and Plate Interactions in East Asia, American Geophysical Union Geophysical Monograph 27, p. 107–126.

Hanson, G.N., and Kroner, A., 1981, Geochemical constraints on the evolution of the early continental crust [and discussion]: Philosophical Transactions of the Royal Society of London. Series A, Mathematical and Physical Sciences (1934-1990), v. 301, p. 423–442.

Herzberg, C.T., Fyfe, W.S., and Carr, M.J., 1983, Density constraints on the formation of the continental Moho and crust: Contributions to Mineralogy and Petrology, v. 84, p. 1–5.

Horwitz, E.P., Chiarizia, R., and Dietz, M.L., 1992, A novel strontium-selective extraction chromatographic resin: Solvent extraction and ion exchange, v. 10, p. 313–336.

Houseman, G.A., McKenzie, D.P., and Molnar, P., 1981, Convective instability of a thickened boundary layer and its relevance for the thermal evolution of continental convergent belts: Journal of Geophysical Research, v. 86, p. 6115–6132.

Hsu, K.J., Wang, Q.C., Li, L., and Hao, J., 1991, Geologic evolution of the Neimonides —a working hypothesis: Eclogae Geologicae Helvetiae, v. 84, p. 1–31.

Jiang, N., Liu, Y., Zhou, W., Yang, J., and Zhang, S., 2007, Derivation of Mesozoic adakitic magmas from ancient lower crust in the North China craton: Geochimica et Cosmochimica Acta, v. 71, p. 2591–2608.

Johnson, M.E., Rong, J., Wang, C., and Wang, P., 2001, Continental island from the Upper Silurian (Ludfordian Stage) of Inner Mongolia: Implications for eustasy and paleogeography: Geology, v. 29, p. 955–958.

Kaur, I., Mishin, Y., and Gust, W., 1995, Fundamentals of grain and interphase boundary diffusion: New York, John Wiley and Sons, 512 p.

Li, Q.L., Chen, F.K., Yang, J.H., and Fan, H.R., 2008a, Single grain pyrite Rb-Sr dating of the Linglong gold deposit, eastern China: Ore Geology Reviews, v. 34, p. 263–270.

Li, Q.L., Chen, F.K., Li, X.H., Wang, F., and He, H.Y., 2008b, Single grain Rb-Sr isotopic analysis of GA-1550 biotite, LP-6 biotite and Bern-4M muscovite ^{40}Ar-^{39}Ar dating standards: Geochemical Journal, v. 42, p. 263–271.

Li, Y., Zhai, M., Yang, J., Miao, L., and Guan, H., 2003, The mineralization age of Anjiayinzi gold deposit in Chifeng, Inner Mongolia, and its implication to the Mesozoic metallogenetic era: Science in China (Series D), v. 33, p. 960–966.

Liu, W., Siebel, W., Li, X.J., and Pan, X.F., 2005, Petrogenesis of the Linxi granitoids, northern Inner Mongolia of China: constraints on basaltic underplating: Chemical Geology, v. 219, p. 5–35.

Ludwig, K.R., 2001, Isoplot/Ex, rev. 2.49: A Geochronological Toolkit for Microsoft Excel: Berkeley, Berkeley Geochronological Center, 55 p.

Minster, J.F., Birck, J.L., and Allegre, C. J., 1982, Absolute age of formation of chondrites studied by the ^{87}Rb-^{87}Sr method: Nature, v. 300, p. 414–419.

Nakai, S.I., Halliday, A.N., Kesler, S.E., and Jones, H.D., 1990, Rb-Sr dating of sphalerites from Tennessee and the genesis of Mississippi Valley type ore deposits: Nature, v. 346, p. 354–357.

Nelson, K.D., 1992, Are crustal thickness variations in old mountain belts like the Appalachians a consequence of lithospheric delamination: Geology, v. 20, p. 498–502.

Rapp, R.P., Shimizu, N., Norman, M.D., and Applegate, G.S., 1999, Reaction between slab-derived melts and peridotite in the mantle wedge: experimental constraints at 3.8 GPa: Chemical Geology, v. 160, p. 335–356.

Rudnick, R.L., Mclennan, S.M., and Taylor, S.R., 1985, Large ion lithophile elements in rocks from high-pressure granulite facies terrains: Geochimica et Cosmochimica Acta, v. 49, p. 1645–1655.

Salters, V.J.M., and Stracke, A., 2004, Composition of the depleted mantle: Geochemistry Geophysics Geosystems, v. 5, p. Q05004, doi: 05010.01029/02003GC000597.

Seedorff, E., Dilles, J.H., Proffett, J.M., Jr., Einaudi, M.T., Zurcher, L., Stavast, W.J.A., Johnson, D.A., and Barton, M.D., 2005, Porphyry deposits: Characteristics and origin of hypogene features: Economic Geology 100th Anniversary Volume, p. 251–298.

Selby, D., and Creaser, R.A., 2001, Re-Os Geochronology and systematics in molybdenite from the Endako porphyry molybdenum deposit, British Columbia, Canada: Economic Geology, v. 96, p. 197–204.

Selby, D., Nesbitt, B.E., Muehlenbachs, K., and Prochaska, W., 2000, Hydrothermal alteration and fluid chemistry of the Endako porphyry molybdenum deposit, British Columbia: Economic Geology, v. 95, p. 183–202.

Sengör, A.M.C., and Natal'in, B.A., 1996, Paleotectonics of Asia: Fragments of a synthesis, *in* Yin, A., and Harrison, M., eds., The tectonic evolution of Asia: Cambridge, Cambridge University Press, p. 486–640.

Shand, S.J., 1943, Eruptive rocks. Their genesis, composition, classification, and their relation to ore-deposits with a chapter on meteorite: New York, John Wiley & Sons, 444 p.

Smoliar, M.I., Walker, R.J., and Morgan, J.W., 1996, Re-Os isotope constraints on the age of Group IIA, IIIA, IVA, and IVB iron meteorites; Science, v. 271, p. 1099–1102.

Steiger, R.H., and Jäger, E., 1977, Subcommission on geochronology: convention on the use of decay constants in geo- and cosmochronology: Earth and Planetary Science Letters, v. 36, p. 359–362.

Streckeisen, A., 1976, To each plutonic rock its proper name: Earth Science Reviews, v. 12, p. 1–33.

Sun, S.S., and Mcdonough, W.F., 1989, Chemical and isotopic systematics of ocean basins: Implications for mantle composition and processes: London, Geological Society of London and Blackwell Scientific Publications, p. 313–345.

Tang, K.D., 1990, Tectonic development of Paleozoic foldbelts at the north margin of the Sino-Korean craton: Tectonics, v. 9, p. 249–260.

Theodore, T.G., Blake, D.W., Loucks, T.A., and Johnson, C.A., 1992, Geology of the Buckingham stockwork molybdenum deposit and surrounding area, Lander County, Nevada: U.S. Geological Survey Professional Paper 798-D, 307 p.

Willigers, B.J.A., Mezger, K., and Baker, J.A., 2004, Development of high precision Rb-Sr phlogopite and biotite geochronology; an alternative to ^{40}Ar/^{39}Ar tri-octahedral mica dating: Chemical Geology, v. 213, p. 339–358.

Wu, F., Sun, D.Y., Li, H.M., Jahn, B.M., and Wilde, S., 2002, A-type granites in northeastern China: age and geochemical constraints on their petrogenesis: Chemical Geology, v. 187, p. 143–173.

Wu, F., Zhao, G., Wilde, S.A., and Sun, D., 2005, Nd isotopic constraints on crustal formation in the North China craton: Journal of Asian Earth Sciences, v. 24, p. 523–545.

Xiao, W.J., Windley, B.F., Hao, J., and Zhai, M.G., 2003, Accretion leading to collision and the Permian Solonker suture, Inner Mongolia, China: Termination of the central Asian orogenic belt: Tectonics, v. 22. doi: 10.1029/2002TC001484.

Xie, X., Yan, M., Li, L., and Shen, H., 1985, Usable values for Chinese standard reference samples of stream sediments, soils, and rocks: GSD 9-12, GSS 1-8 and GSR 1-6: Geostandards Newsletter, v. 9 p. 277–280.

Xu, J., Shinjo, R., Defant, M.J., Wang, Q., and Rapp, R.P., 2002, Origin of Mesozoic adakitic intrusive rocks in the Ningzhen area of east China: Partial melting of delaminated lower continental crust?: Geology, v. 30, p. 1111–1114.

Yang, J., and Zhou, X., 2001, Rb-Sr, Sm-Nd, and Pb isotope systematics of pyrite: Implications for the age and genesis of lode gold deposits: Geology, v. 29, p. 711–714.

Yang, J., Wu, F., Wilde, S.A., Chen, F., Liu, X.M., and Xie, L., 2008, Petrogenesis of an alkali syenite-granite-rhyolite suite in the Yanshan fold and thrust belt, Eastern North China craton: Geochronological, geochemical and Nd-Sr-Hf isotopic evidence for lithospheric thinning: Journal of Petrology, v. 49, p. 315–351.

Zartman, R.E., and Doe, B.R., 1981, Plumbotectonics—the model: Tectonophysics, v. 75, p. 135–162.

Zhang, S.H., Zhao, Y., and Song, B., 2006, Hornblende thermobarometry of the Carboniferous granitoids from the Inner Mongolia Paleo-uplift: Implications for the tectonic evolution of the northern margin of North China block: Mineralogy and Petrology, v. 87, p. 123–141.

Zhang, S.H., Zhao, Y., Song, B., Yang, Z.Y., Hu, J.M., and Wu, H., 2007, Carboniferous granitic plutons from the northern margin of the North China block: Implications for a late Palaeozoic active continental margin: Journal of the Geological Society, London, v. 164, p. 451–463.

Zhang, S.H., Zhao, Y., Song, B., Hu, J.M., Liu, S.W., Yang, Y.H., Chen, F.K., Liu, X.M., and Liu, J., 2009, Contrasting Late Carboniferous and Late Permian-Middle Triassic intrusive suites from the northern margin of the North China craton: Geochronology, petrogenesis and tectonic implications: Geological Society of America Bulletin, v. 121, p. 181–200.

Zheng, J., Griffin, W.L., O'Reilly, S.Y., Lu, F., Yu, C., Zhang, M., and Li, H., 2004, U-Pb and Hf-isotope analysis of zircons in mafic xenoliths from Fuxian kimberlites: Evolution of the lower crust beneath the North China craton: Contributions to Mineralogy and Petrology, v. 148, p. 79–103.

Zhou, X., Sun, M., Zhang, G., and Chen, S., 2002, Continental crust and lithospheric mantle interaction beneath North China: Isotopic evidence from granulite xenoliths in Hannuoba, Sino-Korean craton: Lithos, v. 62, p. 111–124.